Development of pre-conceptual ITER-type ICRF antenna design for DEMO

PAPER • OPEN ACCESS

Development of pre-conceptual ITER-type ICRF antenna design for DEMO

OPEN ACCESS
IOP Publishing | International Atomic Energy Agency Nuclear Fusion
Nucl. Fusion **61** (2021) 046039 (14pp) https://doi.org/10.1088/1741-4326/abe7d0

Development of pre-conceptual ITER-type ICRF antenna design for DEMO

V. Bobkov[1,*], M. Usoltceva[1], H. Faugel[1], A. Kostic[1], R. Maggiora[2], D. Milanesio[2], V. Maquet[3], R. Ochoukov[1], W. Tierens[1], F. Zeus[1] and W. Zhang[1]

[1] Max-Planck-Institut für Plasmaphysik, 85748 Garching, Germany
[2] Politecnico di Torino, Italy
[3] Laboratory for Plasma Physics, ERM-KMS, TEC Partner, 1000 Brussels, Belgium

E-mail: volodymyr.bobkov@ipp.mpg.de

Received 22 December 2020, revised 2 February 2021
Accepted for publication 18 February 2021
Published 22 March 2021

Abstract

ICRF antenna development for DEMO for the pre-conceptual phase is carried out by merging the existing knowledge about multi-strap ITER, JET and ASDEX upgrade antennas. Many aspects are taken over and adapted to DEMO, including the mechanical design and RF performance optimization strategies. The minimization of ICRF-specific plasma-wall interactions is aimed at by optimizing the feeding power balance, a technique already proven in practice. Technological limits elaborated for the components of ITER ICRF system serve as a guideline in the current design process. Several distinctive aspects, like antenna mounting, integration with the neighboring components or adaptation for neutron environment, are tackled individually for DEMO.

Keywords: ICRF antenna, DEMO, DEMO heating system, ICRF heating

(Some figures may appear in colour only in the online journal)

1. Introduction

ICRF (ion cyclotron range of frequencies) is envisaged as one of the plasma heating solutions for European DEMO studied with the EUROfusion consortium, assuming the core physics studies show that direct ion heating is required during the ramp-up and eventually during the stationary discharge phases. The expected DEMO schedule described in [1] implies that design of the DEMO technical subsystems undergoes several stages from the pre-conceptual to the conceptual, then to the engineering design. The finish of the latter is scheduled after the projected start of the ITER ICRF operation, thus the return-on experience (RoX) from ITER is a significant factor. Therefore, designing a DEMO ICRF antenna with ITER-like elements or of 'ITER type' allows RoX in many areas, e.g. in high RF power density ICRF operation in nuclear environment, power coupling, matching, control of the feeding parameters, reliability etc.

The work presented here covers the first steps, started in 2019, toward the pre-conceptual design of the 'ITER-type' in-port multi-strap ICRF antenna for DEMO. The antenna is being developed and optimized with an emphasis on compatibility with the power requirements of ∼50 MW coupled ICRF power out of the total planned heating and current drive power of ∼130 MW [2] and with a high-Z first wall. ICRF power can thus be a large fraction of the total requested heating power. This makes solving the ICRF power coupling issue essential, and that depends critically on the area of the ICRF antenna(s) can cover at the first wall. Release of impurities at the high-Z first wall by the ICRF sheath driven plasma-wall interactions (PWIs) needs to be minimized in parallel. For the low-Z first wall components, although unlikely to be mounted in DEMO, lifetime limitations due to enhanced sputtering require the PWI minimization as well. The following antenna development aspects are under focus:

* Author to whom any correspondence should be addressed.

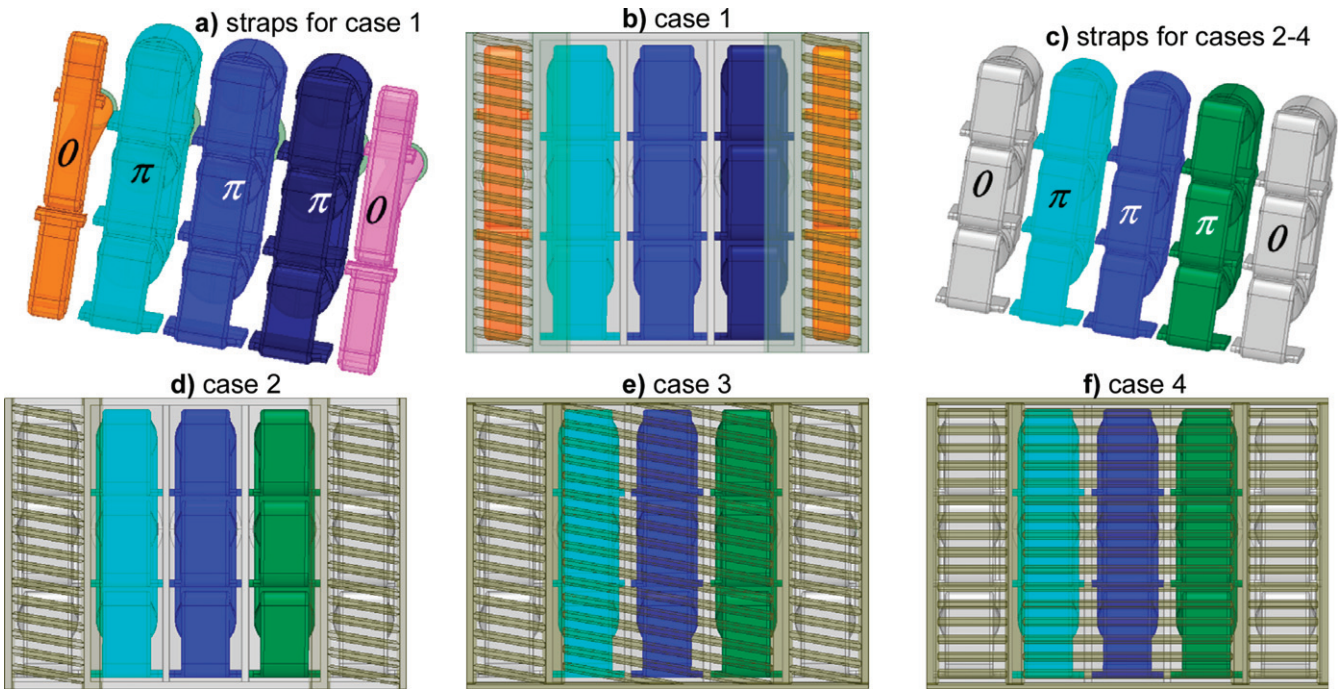

Figure 1. 5-strap setup and corresponding antenna configurations.

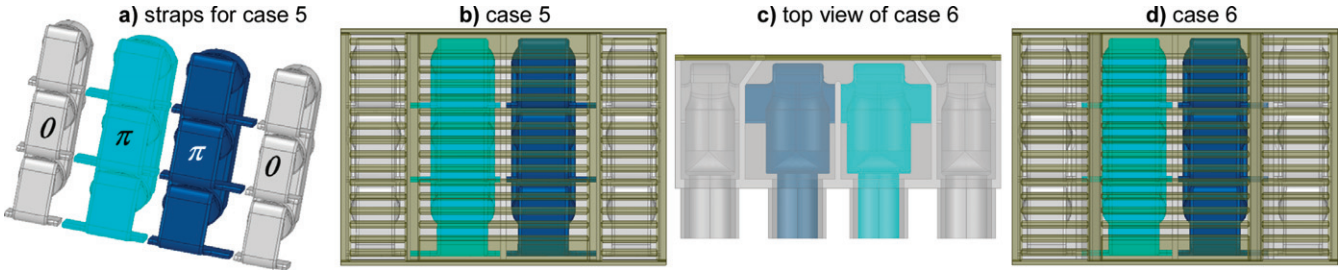

Figure 2. 4-strap setup and corresponding antenna configurations.

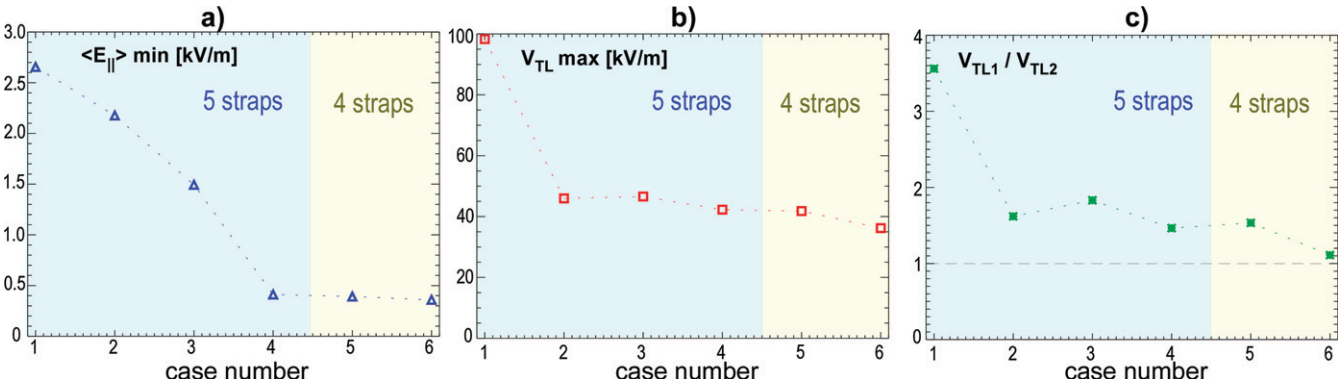

Figure 3. Summary of analysis of cases 1–6: (*a*) minimum of averaged $E_{||}$ near field (normalized to 1 MW), (*b*) maximum voltage in TL, (*c*) voltage balance ratio.

- Performance, i.e. the amount of coupled power, minimization of the image currents on the antenna and its vicinity, control of the maximum voltages in the feeding lines, optimization of the power spectrum;
- Mechanical aspects, i.e. feasibility of antenna manufacturing, procedures of the antenna installation through the port, vacuum windows at the back of the port.

The first part of this work is focused on exploring the antenna strap geometries and feeding mixes for a poloidal half of the antenna, while defining the boundary conditions for the antenna integration. The geometry of a single strap, while not copied from ITER, is similar to the ITER antenna geometry—triplets connected to 4-point-junctions (4PJ). The width, length and depth of the straps are optimized in steps; variations

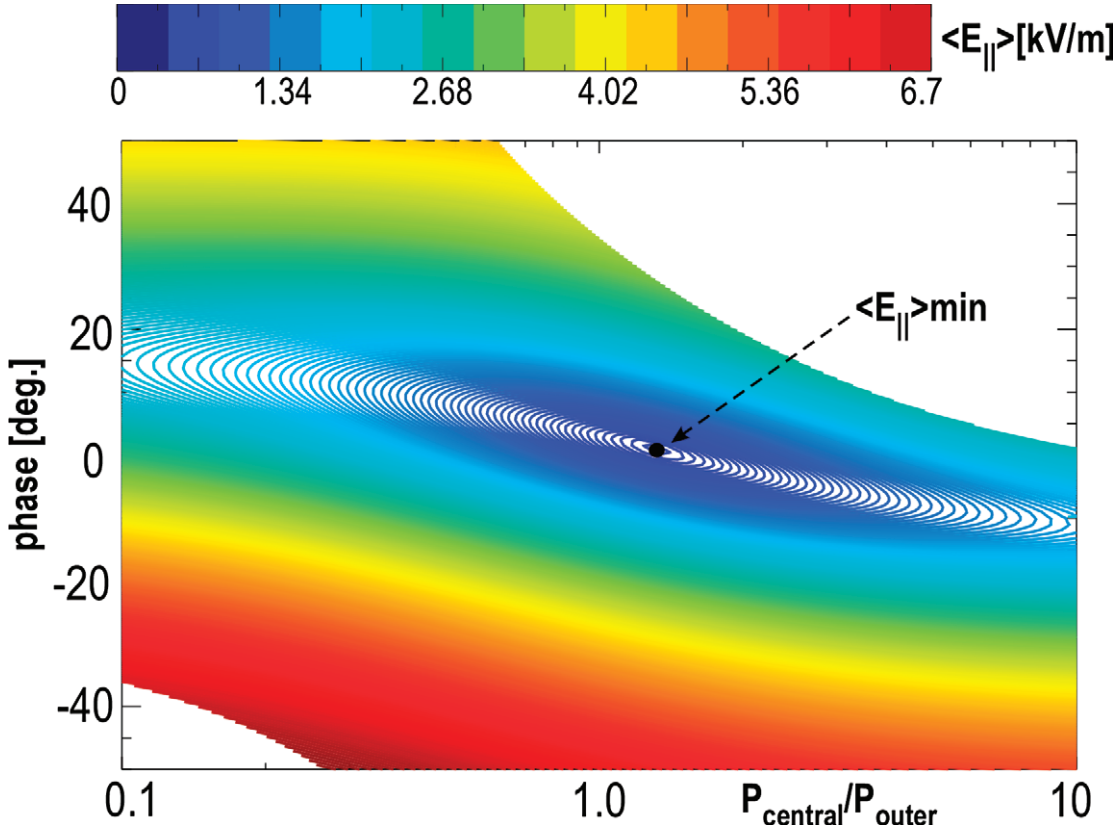

Figure 4. Case 6: $\langle E_{||} \rangle$ (normalized to 1 MW) as a function of power balance and deviation from the standard phasing.

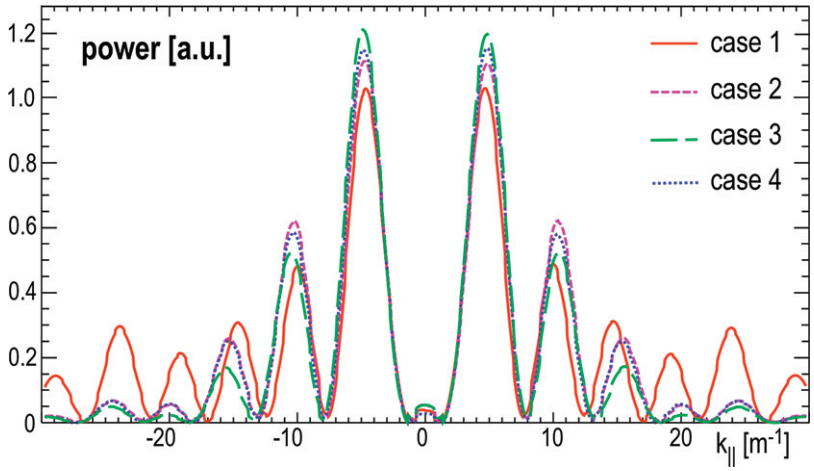

Figure 5. Power spectrum of toroidal RF magnetic field as a function of $k_{||}$ for the cases of 5-strap configuration.

of the toroidal number of straps and the geometry of the Faraday screen (FS) as well as septa between the straps are also studied.

In the second part of the work, further antenna modifications are assessed including those which make the integration of the antenna in the port possible. The antenna port has to penetrate through the breeding-blanket (BB). The mechanical integrity of the BB back supporting structure allows only a limited toroidal extension of the port. At the same time, a cut-out of the front BB structure (the breeding zone) is of consideration, in order to provide additional toroidal extension. For an efficient usage of space, these boundary conditions imply that the antenna structure includes routing of the feeding lines and alignment of antenna halves. Results of such optimization according to the aspects listed above are shown in sections 2 and 3.

Basic extrapolations show that it is not feasible to design an ICRF antenna for DEMO with a size limited by the port size of 1.1 m $\times$ 2.8 m, defined the projected dimensions of the DEMO limiter port. A surface area of $\sim$4 m^2 or larger and the sufficiently low dominant contribution of parallel wave number spectrum $|k_{||}|$ below 6 m^{-1} are required to couple the power of $\sim$16 MW per antenna for the total of $\sim$50 MW with 3 antennas. Therefore, the antenna geometries explored in this

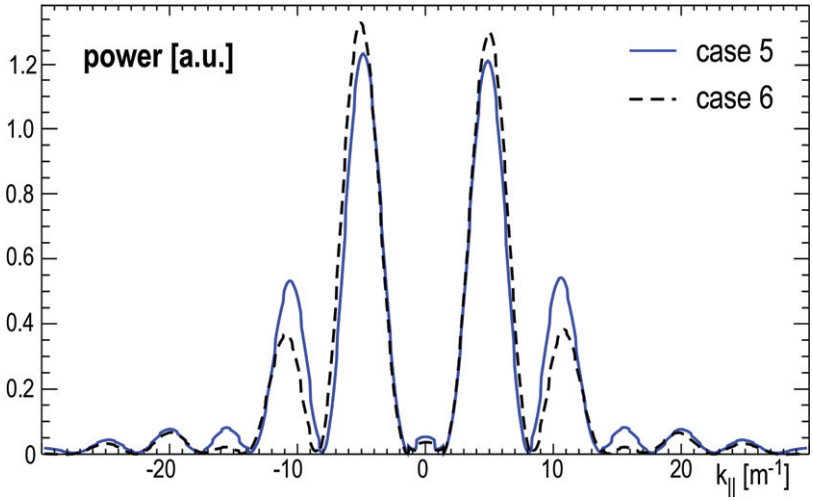

Figure 6. Power spectrum as a function of $k_{||}$ for 4 strap configurations.

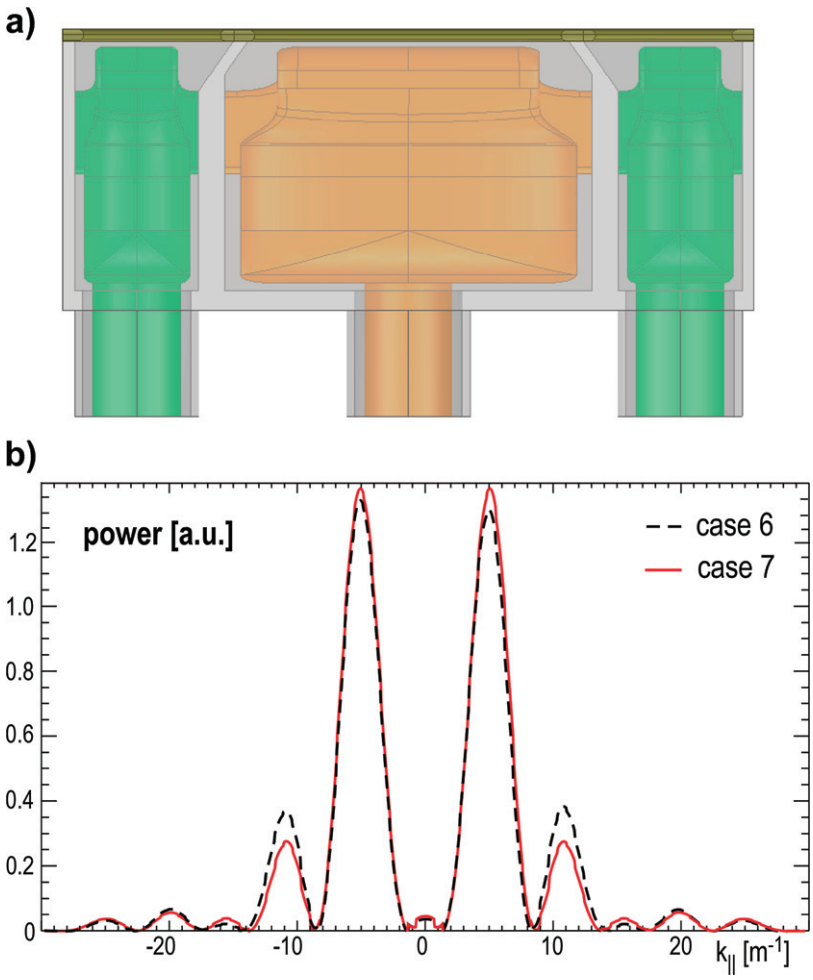

Figure 7. Case 7: (*a*) 3-strap antenna geometry, top view, (*b*) comparison of $k_{||}$ spectrum to case 6.

paper have the dimensions bigger than the port size. Instead of a straight installation in one piece it is proposed to install them in two separate halves. The available port dimensions are used to the maximum, in order to increase the area of the antenna, especially its toroidal extent. The procedures of antenna installation for 2 different options are provided in section 4. It is pointed out that an interaction with the EUROfusion WPBB (work package breeding blanket) team is required, because the antenna toroidal extension larger than the port size implies partial cut-outs of the breeding zone of the blanket.

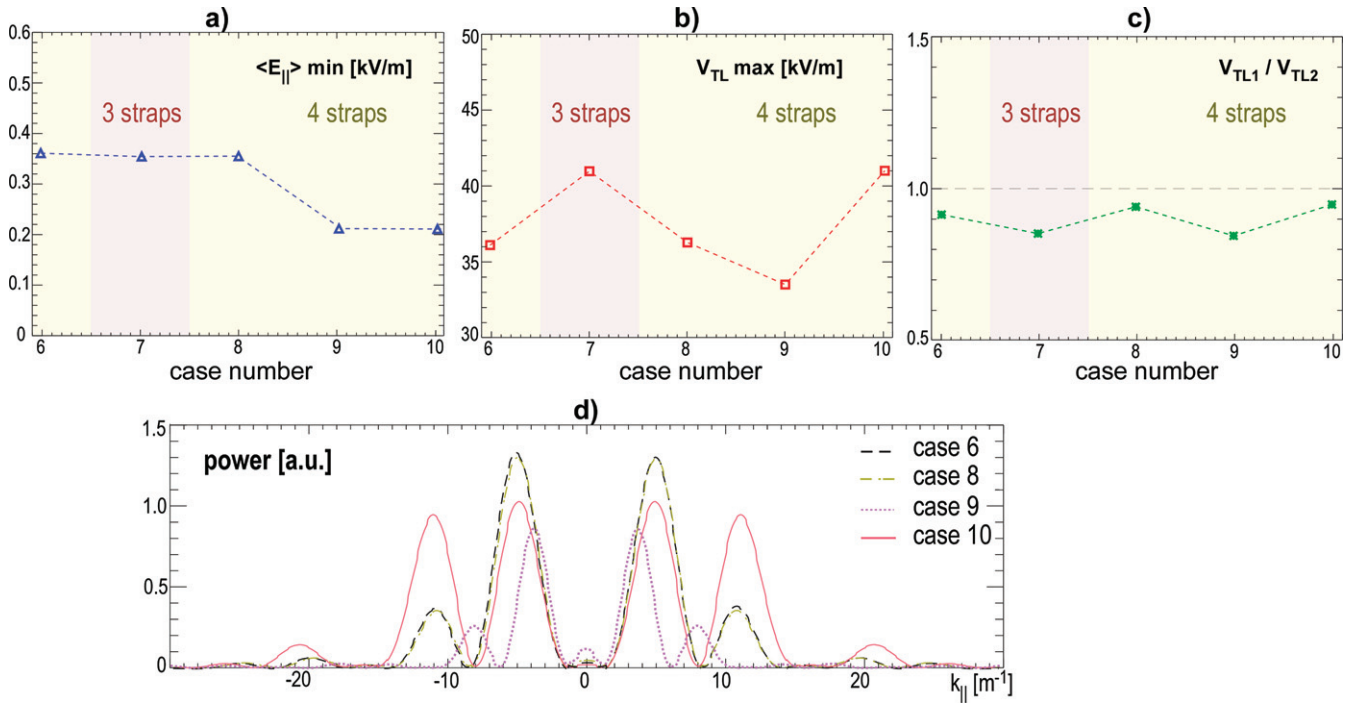

Figure 8. Summary of analysis of cases 6–10: (*a*) minimum of averaged $E_{||}$ near field (normalized to 1 MW), (*b*) maximum voltage in TL, (*c*) voltage balance ratio, (*d*) $k_{||}$ spectrum.

2. Exploration of geometries

An initial assessment of performance of several strap configurations was performed aimed at using an ITER-type ICRF antenna for plasma heating, minimizing RF specific PWIs and maximizing the coupled power. In order to improve flexibility of integration of the antenna into DEMO in the future and to simplify the first step of the studies, the ITER-type antenna was divided in two poloidally arranged halves (PAH); the first part of the geometry exploration is done using one half only. The frequency was fixed to 53 MHz assumed to be a middle-range representative of the operating frequencies for heating scenarios currently considered for DEMO. Geometrical options for antenna configurations were studied, mainly taking into account three aspects as follows:

(a) Cancellation of the image currents on the lateral antenna boundaries, in order to minimize the parallel RF electric field $E_{||}$ at the antenna ($E_{||}$ near field). This aims at minimizing the PWI caused by the RF sheath rectification mechanism in antenna vicinity and on the field lines connections to the antenna [3, 4].

(b) For a fast wave antenna, minimized $E_{||}$ near field has a rather small contribution to the total launched RF power. The power is predominantly carried by the parallel RF magnetic field and perpendicular RF electric field which launch the fast wave. Generally, the antenna power spectrum should be optimized independently of $E_{||}$ near the antenna, in order to minimize the effect of unabsorbed or uncoupled RF power in the edge, in particular in the scrape-off layer (SOL). This RF power can lead to appearance of the far-fields including $E_{||}$ and PWI remote w.r.t. the antenna. In order to avoid unabsorbed power in the core [5] and excitation of the coaxial modes [6], low $k_{||}$ ($|k_{||}| < k_0$, where k_0 is the vacuum propagation constant) contributions need to be minimized, i.e. $k_{||}$ should be higher than few k_0. To avoid additional power circulating in the edge due to poor coupling to the plasma, the contributions at high $k_{||}$ need to be avoided. At the same time, to maximize the RF power coupled by the ITER-type antenna, the lowest possible $k_{||}$ is favourable. The target value of $|k_{||}| = 4$–5 m^{-1} is considered as a compromise for the dominant wave number under the geometrical boundary conditions and is well suitable for ion heating by ICRF in DEMO [5, 7]. The contributions at lower and at higher $k_{||}$ are aimed to be minimized.

(c) The equal maximum voltages in the transmission lines (TL) of the antenna feeders and maximized coupled power are aimed for, under the feeding conditions corresponding to the optimized near fields and the antenna spectrum.

2.1. 4- and 5-strap antennas

Based on the previous experience with the 3-strap antennas in ASDEX upgrade [3, 4], the near field calculations for the ITER antenna and on the aspects of RF power absorption at low $k_{||}$, the symmetric dipole phasing (0—…—π—…—0) was chosen as the most promising feeding scheme to satisfy the properties described above. In order to describe the power balance, P_{central} is used for the total power launched by central strap(s) and P_{outer} is used for the power launched by both outer straps. Figure 1 shows configurations with 5 toroidally distributed straps, whereas figure 2 shows the setup

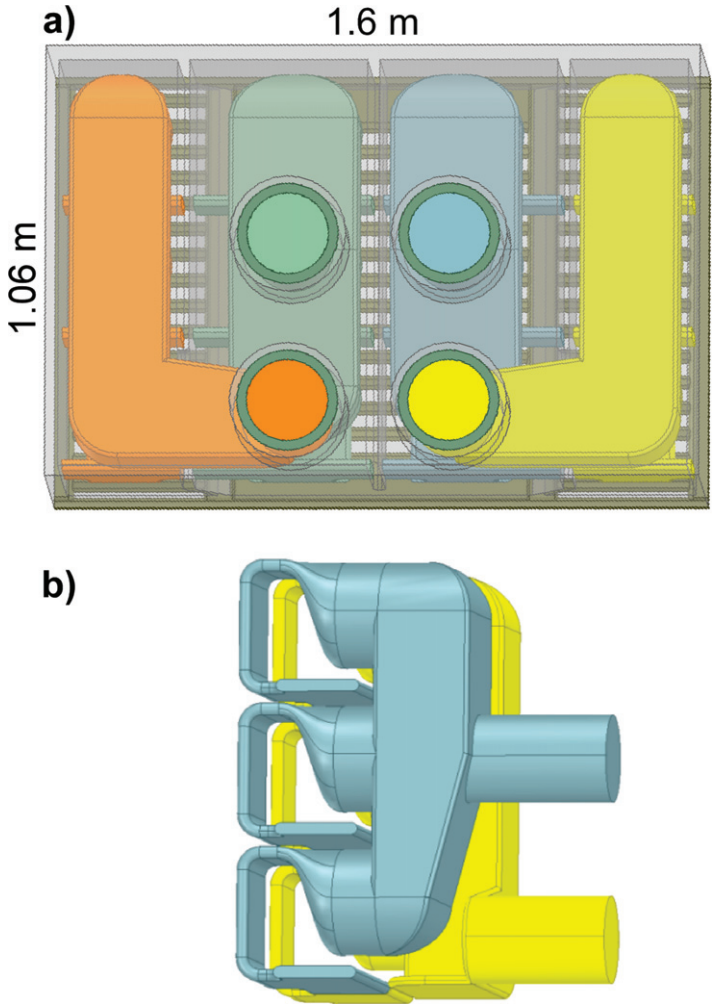

Figure 9. Case 8 antenna (case 6 with rerouted feeders): (*a*) back view, (*b*) side view of two adjacent straps.

with 4 straps. For the antenna with 5 straps, options with various shapes of the straps (case 1) and the partial opening in the FS (cases 1 and 2) in the central area of the antenna, as well as the options with continuous FS (cases 3 and 4) were considered. Two 4-strap configurations were assessed, with the latest one (case 6) being the most promising candidate for continuing the development. With the exception of the toroidal/poloidal dimensions of case 1 of 1.27 m × 1.6 m, the dimensions of the antenna box for all the cases were fixed to 1.14 m × 1.58 m.

HFSS (High Frequency Structure Simulator) software was used to model the ICRF antenna cases. A conducting dielectric (salt water) was placed in front of the antenna to serve as a loading. While this setup does not provide accurate absolute values for the load impedance and power absorption, it is sufficient to compare relative performance of various designs. The procedure to compare the RF performance of various geometries is applied as follows:

(a) A feeding scan of the $P_{\text{central}}/P_{\text{outer}}$ and the phasing in the proximity of the default dipole phasing provides an optimum that corresponds to a minimum of the parallel RF electric field $E_{||}$ on the antenna lateral sides.

(b) The maximum voltage in the TL V_{TL} is calculated for 8 MW input power per antenna half (yielding the total ICRF power of about 50 MW, assuming that three DEMO ports can be allocated for ICRF system), using the found optimum feeding. The absolute values are taken only as a rough approximation.

(c) The $k_{||}$ spectrum for the optimum feeding is evaluated for two requirements: (i) to have the main component close to 4–5 m^{-1}; (ii) to avoid large secondary peaks. The calculations of $k_{||}$ used in this paper are based on the toroidal RF magnetic field.

Figure 3 presents the results of the analysis of these cases: (a) value of $E_{||}$ field averaged close to the antenna lateral sides (along the whole height where presumably the antenna plasma-facing components will be located) at the optimum feeding, referred to as the minimum field $\langle E_{||}\rangle_{\text{min}}$, (b) the transmission line voltage V_{TL} and (c) the voltage balance ratio between the outermost left strap and the neighboring strap $V_{\text{TL1}}/V_{\text{TL2}}$. The result of feeding scan for case 6 is shown in figure 4, as a function of the power balance ($P_{\text{central}}/P_{\text{outer}}$, x-axis) and a small phasing deviation from the default symmetric dipole phasing (y-axis). We aim to minimize the figures of merit shown in figures 3(*a*) and (*b*)

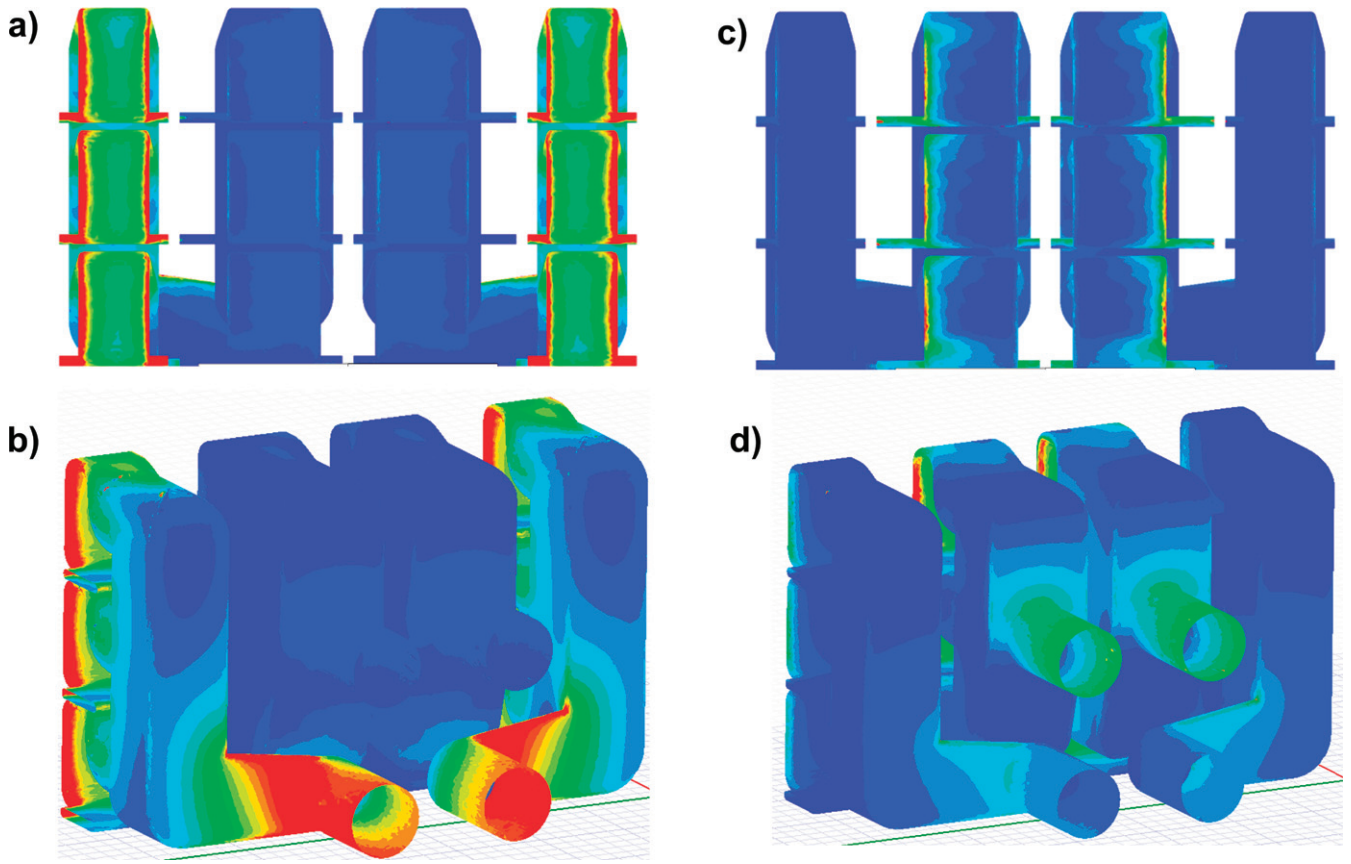

Figure 10. Case 8: I_{surf} distribution for case 8: (*a*) and (*b*) (1, 0, 0, 1) straps excitation, (*c*) and (*d*) (0, 1, 1, 0) straps excitation.

and bring the voltage balance shown in figure 3(*c*) close to unity.

Case 1 was inspired by previous results, which showed that in the so-called JET A2 antenna, the central straps can be efficient in the near-field excitation at the lateral side of the antennas than the central straps in the ITER antenna [8]. In the current work, the combination of the geometry of the central straps similar to those of the ITER antenna and the geometry of the outer straps similar to the JET A2 antenna central straps showed very high excited $\langle E_{||}\rangle_{\min}$ and very high and misbalanced V_{TL}. This demonstrates that any antenna should be considered as a whole, and not a superposition of the components. In addition, more recent calculations show that the combination of the imprecise near-field normalization in the past simulations and the difference in the shape of the A2 antenna straps was artificially enhancing the effect of the A2 antenna central straps on $E_{||}$.

Cases 2–4 show that having a more homogeneous setup for the straps as well as continuous and left/right symmetric horizontal FS favors lower $\langle E_{||}\rangle_{\min}$ for such relatively broad antenna. It was checked that the full FS in case 3 is beneficial for the $\langle E_{||}\rangle$ minimization compared to the partially open FS in case 2. In addition, the $k_{||}$ power spectrum is improved (according to the criteria listed above), as can be seen in figure 5. The simultaneous improvement of $k_{||}$ can be explained by the fact that the minimization of the image currents at the lateral sides of the antenna is beneficial both for the $E_{||}$ near field and for the purity of the spectrum. However it should be reminded, that $E_{||}$ does not usually carry significant RF power. Generally, the analysis of the near field and the analysis of the power spectrum are complementary to each other.

A detailed analysis of the RF power circulation for every strap reveals that for the most central strap in the 5-strap configurations, the net power delivered to the plasma is small. This explains why, while going from the 5-strap configuration (case 4) to the 4-strap configuration (case 5), the maximum voltages in the TL do not increase. Furthermore, by introducing a shaped septum between the central and the outer straps in case 6, it is possible to decrease $\langle E_{||}\rangle_{\min}$ further and to bring the voltage balance close to 1. This also coincides with a further improvement of the $k_{||}$ power spectrum which is shown in figure 6.

2.2. 3-strap antenna

Before continuing the development of the rather successful 4-strap configuration ‘case 6’, a possibility was tested to further reduce the number of straps to 3 (figure 7), therefore also reducing the number of feeding lines and the complexity of the whole system. The significance of the effect of the cross-coupling between the central straps on the coupled power, as observed with the 5-strap design, was also checked.

The 3-strap antenna (figure 7(*a*)) is a modification of ‘case 6’ antenna. A wide inner strap replaces the previous 2 central straps and the septa are made thicker to increase the mechanical stability. The central 4PJ width was maximized to ensure high capacitance and therefore low characteristic

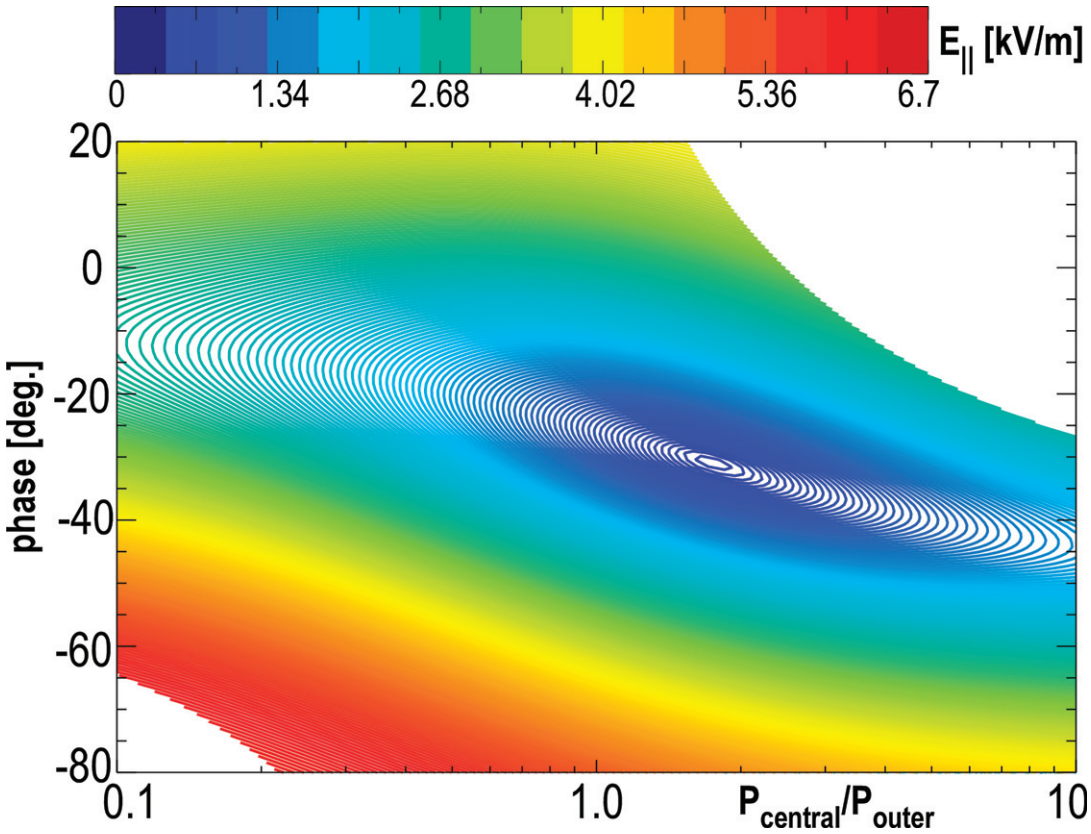

Figure 11. Case 8: $\langle E_{||} \rangle$ (normalized to 1 MW) as a function of power balance and deviation from the standard phasing.

impedance, same as was done in all other cases. High characteristic impedance of the components at these locations is undesirable, since it can increase the power reflection coefficient on the generator side of 4PJ, and hence increase V_{TL}. At the same time, a minimum gap size between conducting surfaces should be obeyed to prevent excessive electric fields and arcing, so the size and relative locations of 4PJs and septa should be optimized. The resulting $k_{||}$ spectrum is not very different from the case 6 (figure 7(*b*)) and the minimum of the near field $E_{||}$ is nearly the same (figure 8(*a*)), but the voltages in the TL V_{TL} are increased (figure 8(*b*)) from the maximum of 36 kV to 41 kV for the same 8 MW coupled power. This leads to a conclusion that for the geometries considered, the 4-strap antenna indeed benefits from having one more strap and one more transmission line to feed it. Though some negative effect from the cross-talk between the 2 central straps always exists, it is not as significant as for the central strap of the 5-strap model. Further modifications could be done to the 3-strap 'case 7' model to better balance the TL voltages, but the 4-strap antenna 'case 6' model clearly surpass it in performance. The potentially attractive hypothetical option of fitting the 3-strap antenna into the 1.08 m wide port is therefore unlikely to be successful, because the $|k_{||}|$ values for the (0–π–0) phasing would be significantly higher than $|k_{||}| = 6\ \mathrm{m}^{-1}$, resulting in excessive V_{TL}.

3. Improvements of 4-strap antenna

As concluded from the previous studies of the considered geometries, the 5-strap and 3-strap antennas do not show advantages over options with 4 straps in the considered feeding schemes and are thus excluded from further considerations. The FS options such as a partial FS and FS aligned with the background magnetic field were tested and showed worse performance than the horizontal FS. The horizontal FS is therefore kept in all following models. Shaped (partially tilted) septa between the outer and the inner straps help considerably in balancing the transmission line voltages and in shaping the spectrum, thus these are used in the next models.

With the exception of one very last model, all other geometries also represent one poloidal half of a full antenna. The effect of the possible poloidal $+90^{\circ}$ phasing has not been studied so far. All the models are left/right symmetric and only the symmetric dipole phasing (0—…—π—…—0) is used as the most promising feeding scheme to satisfy the heating requirements. The same optimization procedure is applied as described in section 2.1.

3.1. Feeders routing

One of the crucial next steps is the rerouting of the antenna feeders. Since the antenna is wider than the port, as was

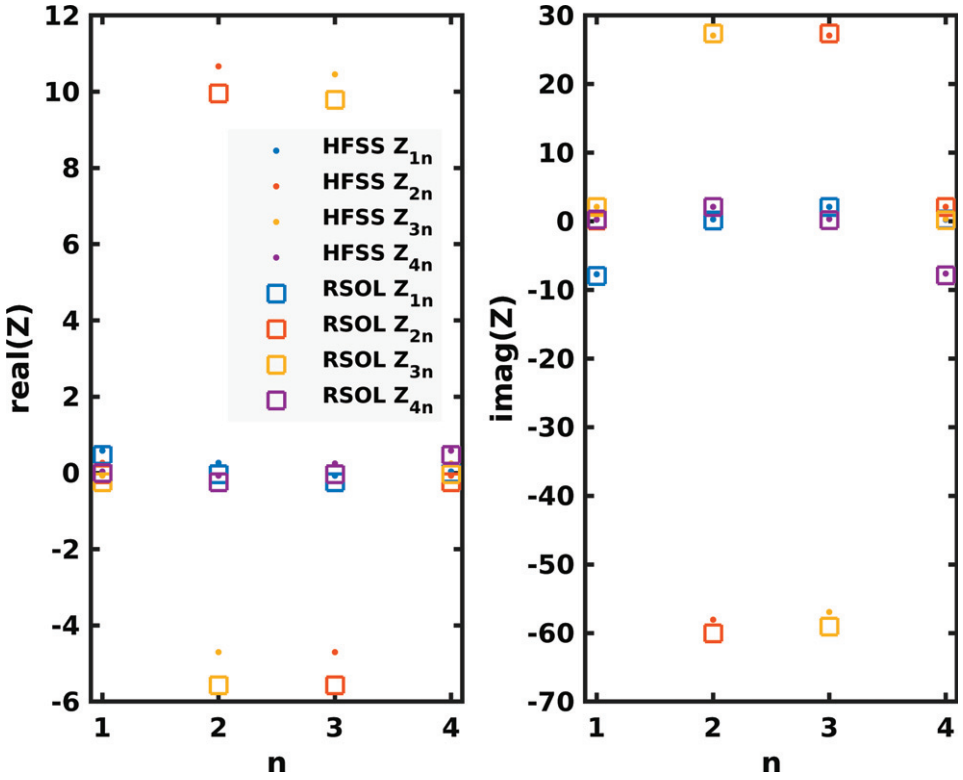

Figure 12. Comparison of Z-matrix elements between HFSS and RAPLICASOL (labeled RSOL) set up with lossy dielectric (sea water) loading.

explained in the introduction, the TL of the outer straps would not fit in the port in the current antenna configuration (see also section 4). The feeders must be shifted toward the center. Figure 9 represents a new 4-strap 'case 8' antenna geometry made in CATIA where the outer triplets have a strip-line connection from the 4PJ to the coaxial lines. The strip-line rerouting has been previously successfully applied in many other ICRF antennas including those at ASDEX upgrade. The lower and upper coaxial lines are at the same toroidal location now and their total toroidal size is 0.67 m which is smaller than the assumed port size.

Note that the central 4PJs had to be modified to free space for the strip-lines. The lower part was made oblique (figure 9(*b*)). Despite the mentioned modifications the distribution of surface current (I_{surf}) on the straps of each triplet is homogenous (see figure 10). This means that such 4PJ is quite insensitive to these details. Equal current distribution is important for maximizing the power coupling efficiency and the poloidal homogeneity of the spectrum. Another issue is that the proximity of the conducting surfaces of the inner and outer straps parts in this model could lead to significant current excitation by neighboring straps. In the previous designs, the straps were always separated by septa, but in this case the septa had to be cut for rerouting. Nevertheless, as seen in figure 10, the cross-talk is kept minor. This was made possible by making the gaps between the conducting surfaces sufficiently large.

The geometry was newly built, but the width of the antenna and the straps themselves were kept nearly the same, as well as the septa tilt angle and the distances between the straps (<1.5% variation). The performance of the rerouted model has not degraded compared to case 6, the spectrum and the TL voltages remain virtually the same (figure 8), even though the height of the antenna was reduced from 1.147 m to 1.060 m (to fit in the port during installation, will be discussed later). The largest difference between case 6 and case 8 is the position of the optimum of the feeding (figure 11), shifted because of the additional electrical length of the outer straps (see case 6 in figure 4).

3.2. *Validation with realistic load*

The RAPLICASOL code recently developed [9] with COMSOL and can cope both with the lossy dielectric and with the (cold) plasma loadings. The code was first tested for the case 8 geometry with the same lossy dielectric loading (sea water) as in HFSS. Figure 12 demonstrates the good agreement between RAPLICASOL and HFSS in terms of complex values of the Z-matrix elements.

The case 8 geometry was then used to obtain reference results with plasma from RAPLICASOL and TOPICA [10] and (about their differences and a benchmark between the two, see [11]). Estimation of maximum voltages in the TL of the feeders based on the pessimistic 'ITER2010low' projected density profile (figure 13) of ITER could be made. A vacuum gap between the antenna and the plasma domain is used to avoid the low-density plasma which is numerically demanding to simulate. The distance from the most protruding antenna part to the coordinate 0 in figure 13 is 10.5 cm and 10 cm from

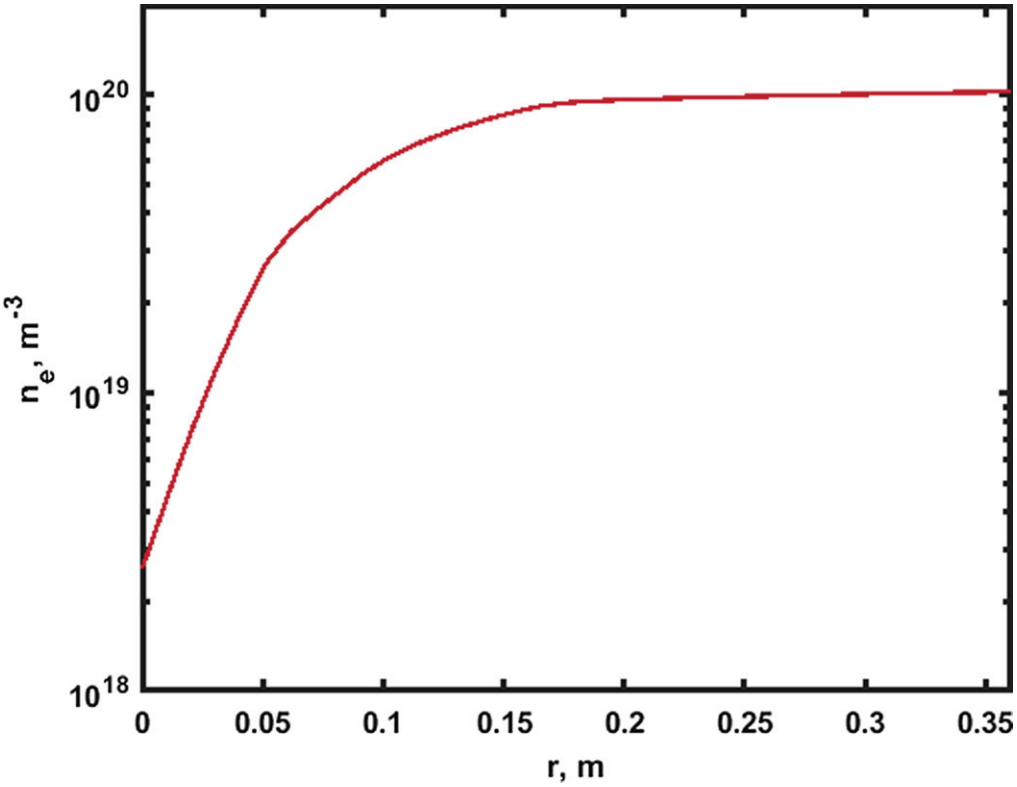

Figure 13. 'ITER2010low' density profile; coordinate 0 corresponds to the start of the plasma domain.

the TOPICA aperture. The large plasma-wall clearance is generally required in ITER and DEMO to reduce the first wall heat fluxes independently of ICRF operation. It is noteworthy however that the density profiles in front of ICRF antennas can be tailored by using local gas injection valves placed close to the antennas, as has been proved experimentally [12] and theoretically [13]. This technique which can improve the coupling and reduce V_{TL} significantly, is planned for ITER [14] and can be similarly implemented in DEMO. The profile given in figure 13 does not include local gas effects.

The feeding parameters for the RAPLICASOL and TOPICA simulations are the optimum parameters provided by the previous HFSS runs. In the RAPLICASOL calculations, a simplification was used for the magnetic field. It was taken as purely horizontal, while in TOPICA it was more realistic, with 15° tilt. This tilt is planned to be included in the next DEMO RAPLICASOL simulations.

The obtained transmission line voltages are shown in figure 14. By a very good agreement of TOPICA and RAPLICASOL, it can be concluded that the HFSS sea water calculations result in voltages about 30% lower than in more realistic plasma modeling. The voltages obtained with the plasma are close to the ITER limit on the TL voltages −45 kV.

This is useful information to guide the HFSS simulations further. The detailed near field analysis with plasma has not been performed yet. A scan of antenna aperture geometry should be made prior to the analysis of the near-fields with plasma loading. In addition, as one of the next steps in the studies, the DEMO plasma profile obtained from the DEMO physics team will be used in the TOPICA and RAPLICASOL calculations.

4. Compatibility with DEMO port

The next step aimed to maximize the antenna dimensions wherever possible and to fit the antenna halves into the port during the installation.

4.1. Poloidally arranged halves (PAH) antenna

First, we describe the suggested installation procedure for the PAH antenna (figure 15(*a*)). The antenna halves are installed one by one, the first half is rotated by 90°, inserted into the vacuum vessel deep enough and rotated back. It is then shifted up as far as the TL allow. In the remaining gap, the second half is introduced in the rotated position, which is then turned back to the normal orientation and installed in its final position. The upper half vertical position is adjusted accordingly (figure 15(*b*)). The halves are attached to each other.

The geometry limits are defined as follows:

- $h_{ant} = l_{port} - l_{gap} \times 2$, so for $d_{port} = 1.1$ m and $l_{gap} = 0.02$ m we can have maximal $h_{ant} = 1.06$ m.
- $l_{ant} = h_{port} - l_{gap} \times 3 - h_{TL}$, so for $h_{port} = 2.8$ m, $l_{gap} = 0.02$ m and $h_{TL} = 0.574$ m the maximum is $l_{ant} = 2.166$ m.

Here h is height (poloidal size), l is width (toroidal size) for antenna (ant), port or TL correspondingly and l_{gap} is the length of a needed clearance between the port walls and the antenna or the antenna halves. $h_{TL} = 0.574$ m is calculated based on the

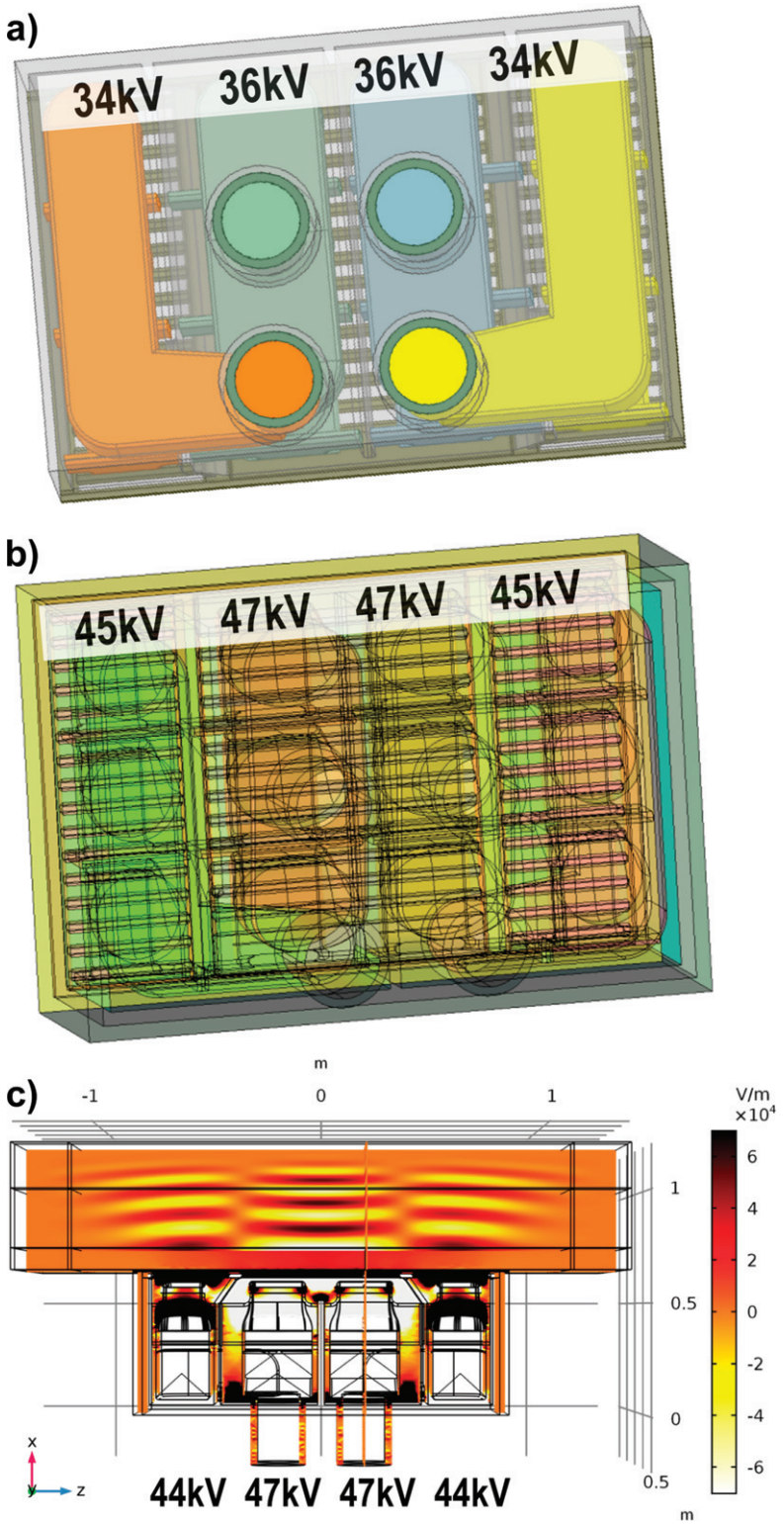

Figure 14. Models for simulations of the reference PAH antenna half, shown with voltages in the transmission lines calculated for 8 MW of power: (*a*) back view of the HFSS model; (*b*) isometric view of the TOPICA model; (*c*) top view of the RAPLICASOL model with radial RF electrical field representing wave propagation in the calculation domain, with septa shape visible.

9-inch (0.229 m) TL having the outer conductor 0.02 m thick and two of them separated vertically by 0.01 m gap. The lower feeder cannot be placed at 0 m from the antenna bottom due to the presence of the bottom wall of the antenna box, so an acceptable shift of 0.026 m from the bottom is assumed.

The antenna dimensions for 'case 8' were increased up to the obtained maximum possible sizes (as derived above), to form the 'case 9' antenna. The model was shortened in the radial direction from 0.615 m in the previous models to 0.527 m, not to protrude further than the breeding zone of

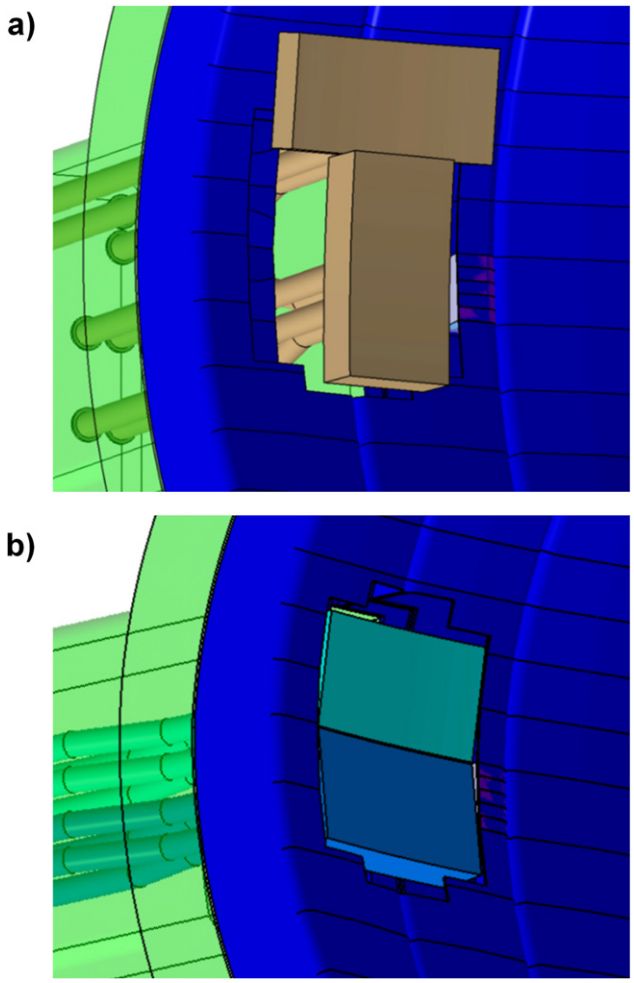

Figure 15. Installation of the PAH antenna: (*a*) first half shifted to let the second half in, (*b*) final position.

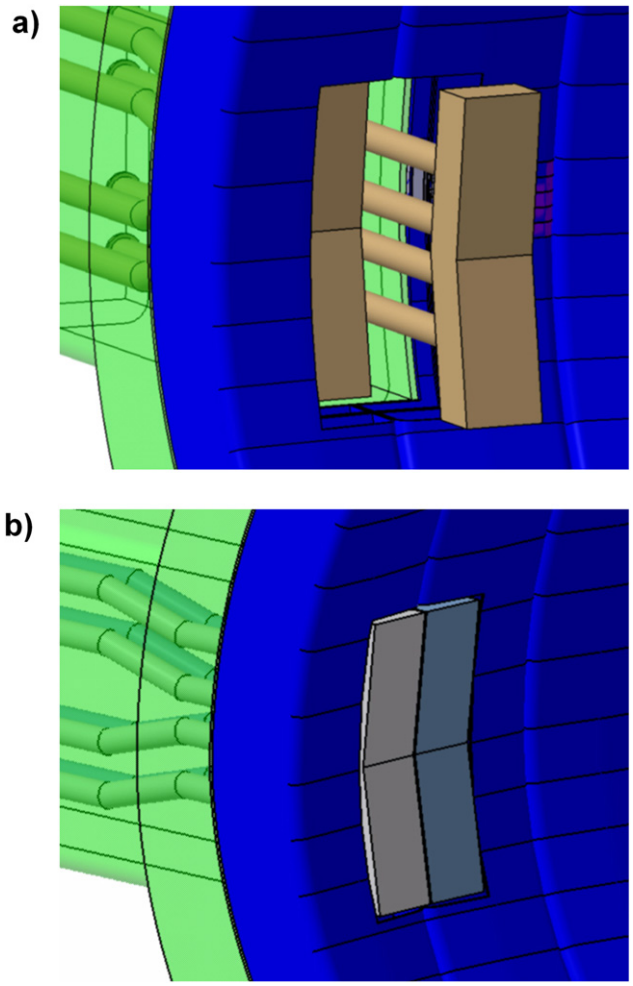

Figure 16. Installation of the TAH antenna: (*a*) first half shifted to let the second half in, (*b*) final position.

the blanket. The analysis of case 9 demonstrates noticeably reduced voltages and lower near field $E_{||}$ in the minimum (figures 8(*a*) and (*b*)), however the V_{TL} balance and spectrum are not properly optimized (figures 8(*c*) and (*d*)), so the design needs further adjustments.

4.2. Toroidally arranged halves (TAH) antenna

In parallel with the PAH antenna, a new approach was developed based on the idea of toroidally arranged halves (TAH) that would not require rotation during installation. The procedure of the assembly is as follows (figure 16(*a*)). One antenna half is introduced to the vessel and shifted to the right as much as the feeders allow. The second half goes through the remaining gap and gets shifted to the left at the end to its final position. Then the right half is shifted to its final position (figure 15(*b*)).

The geometry limits are defined as follows:

- $h_{ant} = h_{port} - l_{gap} \times 2$, so for $h_{port} = 2.8$ m and $l_{gap} = 0.02$ m we can have maximal $h_{ant} = 2.76$ m.
- $l_{ant} = l_{port} - l_{gap} \times 2 - l_{TL}$, so for $l_{port} = 1.1$ m, $l_{gap} = 0.02$ m and $l_{TL} = 0.289$ m the maximum $l_{ant} = 0.771$ m.

$h_{TL} = 0.249$ m is the diameter of a 9-inch (0.229 m) transmission line plus its outer conductor thickness 2×0.02 m and a shift of 0.02 m from the box edge not to interfere with the antenna side wall.

An HFSS model of an example of a TAH antenna with maximized dimensions and the depth of 0.527 m was constructed (figures 17(*a*) and (*b*)) and analyzed (figure 8), as 'case 10'. It would not be useful to analyze only one half in the toroidal direction, so for this case a full antenna with both halves were simulated for the first time. For now, the poloidal phasing of 0° is taken. Good voltage balance between the central and outer straps was obtained (figure 8(*c*)), the same for both upper and lower straps, but the maximum V_{TL} is higher (figure 8(*b*)). However, the voltage can be reduced during the future development, by making the internal structure of the antenna model, in particular septa between the antenna halves, more alike to the PAH antenna models considered so far, e.g. as per comparison of figures 2(*c*) and 17(*a*). The near fields are reduced well (figure 8(*a*)) close to $P_{central}/P_{outer} \approx 0.9$, the region of the decrease is narrower. The central septum reduces the power capability and enhances the secondary peak of the power spectrum (figure 8(*d*)). This design can be further optimized and the next steps are described in [15].

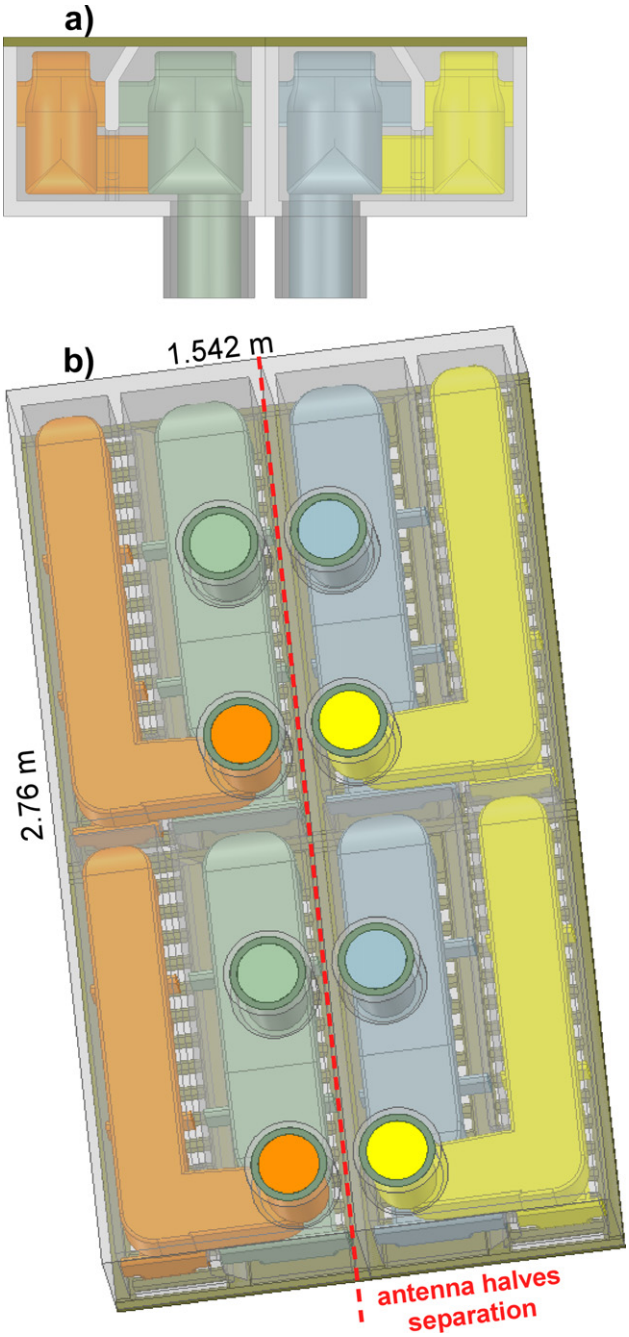

Figure 17. First model of a TAH antenna, case 10: (*a*) top view; (*b*) view from the back.

4.3. Other integration issues

Besides the analysis of various geometries, first steps to prepare the design for neutronics analysis can be seen (figure 18). A bend of TL is introduced to reduce neutron tunneling through coaxial feeders. The remaining infrastructure (supports, cooling, shielding, eventually breeding, etc) and T-stub connections similar to ITER antenna are to be added at the further stages of the antenna concept development, as well as a proper interface with the plasma facing components. Some of the next steps which are being performed are described in [15]. Independently, work has been started to design vacuum windows at the back of the port.

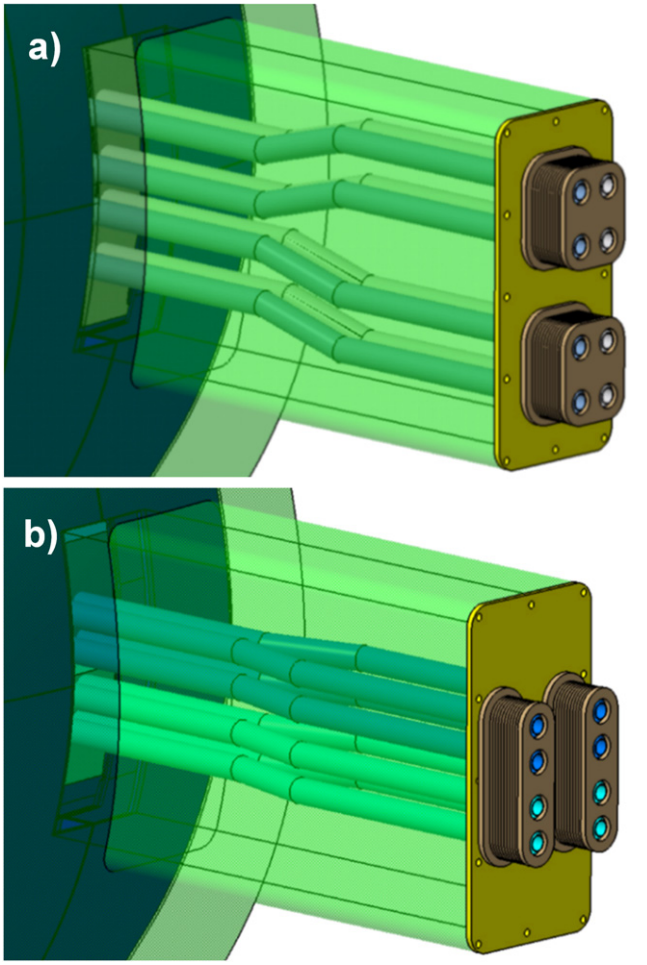

Figure 18. Bend of TLs and vacuum windows for: (*a*) TAH antenna, (*b*) PAH antenna.

5. Conclusions

A design development work has begun for DEMO ICRF antenna and it is currently in progress. The impact of several important details has been evaluated by consecutive steps of improvements and the summary of them was presented. The design of the antenna itself is converging and further steps will be taken in the development of the whole ICRF system, for example.

Two concepts are considered—antenna with PAH antenna and antenna with TAH antenna. Both approaches include taking advantage of a larger toroidal extent than the port size, which would be possible with the provided installation procedure. A cut into the surrounding blanket is required for both concepts and its size limitation will play a crucial role on the achievable antenna extent. Close interaction with the EUROfusion WPBB team is foreseen to define the strategy of antenna integration with the suggested blanket cut.

The antenna front surface areas are similar for the two concepts: 2.166 m $\times$ 2.12 m ($\sim$4.6 m^2) for TAH and 1.542 m $\times$ 2.76 m ($\sim$4.3 m^2) for PAH, meaning similar order of value for the coupled power. The PAH antenna can provide a spectrum with a lower number for the main peak and could be

even considered for a phasing in compact dipole ($0–\pi–0–\pi$). The TL voltages are somewhat lower, which gives a benefit in terms of coupled power. The TAH antenna is much easier in installation and has a smaller impact on the breeding area. It shows good voltage balance and the spectrum with main component within the target range. The secondary peak in the $k_{||}$ spectrum, observed in the first TAH antenna design, needs to be mitigated. This is feasible, as was already observed in the course of previous work, by altering the elements like septa, FS and size of the straps. Both designs have a room for improvement. Overall, the TAH concept looks more promising, provided that the voltage in the transmission line can be decreased. This can be achieved by modifying the antenna internal structure by making more alike to the so far considered PAH antenna models.

The possibility of using 3-strap or 5-strap designs was assessed and these options are abandoned for now due to several complications.

One reference case with plasma was computed using TOPICA and RAPLICASOL and showed TL voltages of the level of ITER (∼45 kV for 16 MW per antenna). The described above advances in the antenna geometry design make it possible to start more detailed studies with plasma loading in the near future. The two tools for plasma simulations are based on different numerical approaches (standalone code TOPICA is based on method of moments, whereas RAPLICASOL is based on the finite element method and written in the COMSOL environment), and therefore provide two independent solutions which can be benchmarked against each other. This allows to obtain higher confidence in the results.

More detailed future studies will also include a more thorough analysis of the $E_{||}$ fields in front of the antenna. For now, only the averaged electric field in the area on the antenna sides is assessed. In addition to that, it should be ensured that there are no local spots with particularly high fields, since the field enhancement leads to extensive non-linear increase in PWIs followed by local antenna damage and plasma contamination.

The further design process will largely involve the ITER return on experience, including the knowledge on thermal and mechanical stability. Further parts of the system behind the antenna front face are in the process of development and/or being adapted from ITER. A first model for the neutronics analysis has been prepared [15]. Results of the Monte Carlo *N*-particle transport code simulations will be reported elsewhere.

Acknowledgments

This work has been carried out within the framework of the EUROfusion Consortium and has received funding from the Euratom research and training program 2014–2018 and 2019–2020 under Grant agreement No. 633053. The views and opinions expressed herein do not necessarily reflect those of the European Commission.

ORCID iDs

V. Bobkov https://orcid.org/0000-0002-2328-9308
M. Usoltceva https://orcid.org/0000-0001-7703-6077
D. Milanesio https://orcid.org/0000-0002-5114-7235
W. Tierens https://orcid.org/0000-0002-6979-8140
W. Zhang https://orcid.org/0000-0002-5951-6779

References

[1] Federici G. *et al* 2019 *Nucl. Fusion* **59** 066013
[2] Franke T. 2019 *Fusion Eng. Des.* **146B** S1642–6
[3] Bobkov V. *et al* 2016 *Nucl. Fusion* **56** 084001
[4] Bobkov V. *et al* 2017 *Plasma Phys. Control. Fusion* **59** 014022
[5] Van Eester D. *et al* 2019 *Nucl. Fusion* **59** 10605
[6] Messiaen A. and Maquet V. 2020 *Nucl. Fusion* **60** 076014
[7] Kazakov Y. *et al* 2021 *Phys. Plasmas* **28** 020501
[8] Bobkov V. *et al* 2019 *Nucl. Mater. Energy* **18** 131–40
[9] Jacquot J. *et al* 2013 *Plasma Phys. Control. Fusion* **55** 115004
[10] Lancellotti V. *et al* 2006 *Nucl. Fusion* **46** S476
[11] Tierens W. *et al* 2019 *Nucl. Fusion* **59** 046001
[12] Jacquet P. *et al* 2016 *Nucl. Fusion* **56** 046001
[13] Zhang W. *et al* 2016 *Nucl. Fusion* **56** 036007
[14] Zhang W. *et al* 2019 *Nucl Mater. Energy* **19** 364–71
[15] Usoltceva M. *et al* 2021 *Fusion Eng. Des.* **165** 112269